TU/e EINDHOVEN UNIVERSITY OF TECHNOLOGY

A Sub-Cycle phase angle distance measure algorithm for power transformer differential protection

Citation for published version (APA):
Tajdinian, M., Samet, H., & M. Ali, Z. (2022). A Sub-Cycle phase angle distance measure algorithm for power transformer differential protection. *International Journal of Electrical Power and Energy Systems*, *137*, Article 107880. https://doi.org/10.1016/j.ijepes.2021.107880

Document license:
CC BY

DOI:
10.1016/j.ijepes.2021.107880

Document status and date:
Published: 01/05/2022

Document Version:
Publisher's PDF, also known as Version of Record (includes final page, issue and volume numbers)

Please check the document version of this publication:

• A submitted manuscript is the version of the article upon submission and before peer-review. There can be important differences between the submitted version and the official published version of record. People interested in the research are advised to contact the author for the final version of the publication, or visit the DOI to the publisher's website.
• The final author version and the galley proof are versions of the publication after peer review.
• The final published version features the final layout of the paper including the volume, issue and page numbers.

Link to publication

General rights
Copyright and moral rights for the publications made accessible in the public portal are retained by the authors and/or other copyright owners and it is a condition of accessing publications that users recognise and abide by the legal requirements associated with these rights.

• Users may download and print one copy of any publication from the public portal for the purpose of private study or research.
• You may not further distribute the material or use it for any profit-making activity or commercial gain
• You may freely distribute the URL identifying the publication in the public portal.

If the publication is distributed under the terms of Article 25fa of the Dutch Copyright Act, indicated by the "Taverne" license above, please follow below link for the End User Agreement:

www.tue.nl/taverne

Take down policy
If you believe that this document breaches copyright please contact us at:

openaccess@tue.nl

providing details and we will investigate your claim.

Download date: 16. Nov. 2023

Electrical Power and Energy Systems 137 (2022) 107880

Contents lists available at ScienceDirect

International Journal of Electrical Power and Energy Systems

journal homepage: www.elsevier.com/locate/ijepes

A Sub-Cycle phase angle distance measure algorithm for power transformer differential protection

Mohsen Tajdinian [a], Haidar Samet [a,b,*], Ziad M. Ali [c,d,*]

[a] Department of Power and Control, School of Electrical and Computer Engineering, Shiraz University, Shiraz, Iran
[b] Electrical Engineering Department, Eindhoven University of Technology, Eindhoven, the Netherlands
[c] College of Engineering, Prince Sattam Bin Abdulaziz University, Wadi Addawaser, KSA, 11991, Saudi Arabia
[d] Electrical Engineering Department, Faculty of Engineering, Aswan University, 81542, Egypt

ARTICLE INFO

Keywords:
Inrush Current
Differential Protection
Power Transformer

ABSTRACT

Power transformer differential protection may confront mal-functioning in authentic discrimination between inrush and internal faults. To tackle the latter mal-functioning, a new two-stages algorithm based on phase content of the current signal of the current transformers (CTs) is put forward. The proposed algorithm is designed based on the fact that the fundamental phase angle of a fault signal ideally remains constant during the fault. However, during inrush cases, the phase angle varies. Also, during the internal fault, the phase angles of the current signals of CTs are in phase while during the external fault, the phase angles of the current signals of CTs are 180° out of phase. In the first stage, the proposed algorithm calculates the fundamental phase angles of the current signals of the CTs using sub-cycle modified recursive least squares (MRLS). Afterward, normalized mean residue (NMR) is employed to measure distance between the estimated phase angles of the CT's currents. MRLS and NMR algorithms require limited samples (i.e. 10 and 5 samples respectively) for executing their calculations. Performance evaluation with simulated and experimental recorded current signals shows the ability of the proposed method in discrimination of the internal faults from inrush and external fault currents.

1. Introduction

Owning to the power transformers being strategic components and also their costliness, differential protection schemes are known as the widely-employed unit protections that play an important role in decreasing the damages of the internal faults [1]. The differential relay operates based on differential currents and due to the power transformer core nonlinearity, large currents may lead differential protection to mal-operation under magnetization inrush currents. The harmonic restrain algorithm is known as the most famous differential protection algorithm that utilizes the harmonic contents of the current signals to discriminate between internal faults and inrush currents [2,3]. However, major challenges including magnetization inrush in low-loss core power transformers, transformer energization with internal fault, internal fault under current transformer (CT) deep saturation, and transformer energization with high remnant flux are the issues that significantly affect the harmonic contents and consequently, the performance of the harmonic restrain algorithm and differential relays.

To deal with internal faults and inrush currents discrimination, several algorithms have been proposed in the literature that tried to introduce signal processing techniques to tackle the aforementioned challenges. These methods consist of determining induced voltage, flux linkage, and instantaneous inductance [4–8], utilizing pattern recognition and fuzzy logic [9–14] and time–frequency analysis [15–19], hybrid ratio-based algorithms [20–22], and employing statistical and similarity indices [23–27].

More or less, these methods have successfully dealt with some of the challenges. However, some restrictions and computationally ineffectiveness of most of these algorithms make them vulnerable and incomprehensive regarding all difficult scenarios. For example, the methods in [4–8] calculate the induced voltage, flux linkage, and instantaneous inductance, and are thus dependent on transformer parameters and require extra accessories such as ssearch coil that make these methods costly. On the other hand, the learning-based methods [9–14] require high memory and training data and also impose a high computational burden if they are to provide good performance. Being sensitive to noise

* Corresponding authors.
E-mail addresses: tajdinian.m@shirazu.ac.ir (M. Tajdinian), samet@shirazu.ac.ir, h.samet@tue.nl (H. Samet), dr.ziad.elhalwany@aswu.edu.eg, dr.ziad.elhalwany@ieee.org, z.ali@psau.edu.sa (Z.M. Ali).

https://doi.org/10.1016/j.ijepes.2021.107880
Received 17 August 2021; Received in revised form 11 November 2021; Accepted 13 December 2021
Available online 23 December 2021
0142-0615/© 2021 The Authors. Published by Elsevier Ltd. This is an open access article under the CC BY license (http://creativecommons.org/licenses/by/4.0/).

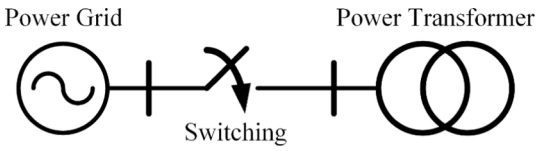

Fig. 1. Single line diagram of a power transformer connected to the power system.

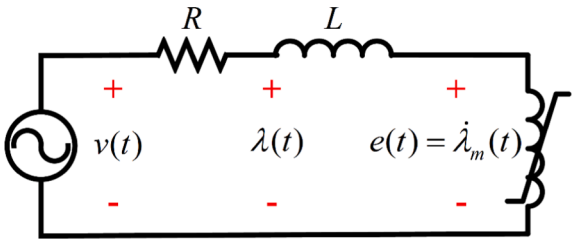

Fig. 2. Equivalent circuit of power transformer after energization.

and requiring a high sampling rate are the drawbacks of the time–frequency based algorithms [15–19]. Ratio-based algorithms [20–22] employ voltage signals as auxiliary information, meaning that these approaches particularly require two potential transformers for implementation. Moreover, these algorithms conduct the calculation based on the discrete Fourier transform that imposes an inherent one-cycle delay to the algorithm. Statistical and similarity-based algorithms [23–27] utilize some characteristics of the signal to find the similarity/dissimilarity of the signal to a standard sinusoidal waveform. It is obvious these algorithms may show vulnerability and sensitivity to the decaying DC and noise components and also deep CT saturation conditions.

To deal with the mal-functioning of the differential protection in the case of inrush currents, this paper introduces an algorithm based on the phase content of the current signals of the CTs. The proposed algorithm is a two-stage framework and is established based on the fast parameter estimation of the current signal. More specifically, the proposed algorithm contains the following contributions:

- The proposed algorithm is based on the fast phase angle estimation of the current signal. It has been shown that the phase angle value for the fault current signal is almost constant while in the case of inrush since the signal does not fit on the conventional waveform of the power system, the phase angle varies during the time. To estimate the phase angle, the proposed method utilizes MRLS which requires 10 samples for executing the calculation to acquire an authenticated phase angle. Note that the signal is sampled with 100 samples/ cycle.
- An index is presented based on the NMR which determines the distance between phase angles of the current signals of the CTs. The distance discriminates the internal faults from inrush current and the external fault signals based on the two assumptions: First, the fundamental phase angle of a fault signal remains almost constant during the fault, while, during inrush cases, the phase angle varies. Second, during the internal fault, the phase angles of the current signals of CTs are in phase while during the external fault, the phase angles of the current signals of CTs are 180° out of phase. Note that the proposed index has the sampling requirements the same as MRLS.
- The proposed method is inherently immune to the internal and external faults accompanied by heavy CT saturation and it does not require extra criterion or calculations to deal with CT saturation.
- Compared with the state-of-the-art, the proposed method has an inherently low computational burden due to the recursive nature of the employed algorithms and calculations.

In the following, section II discusses the proposed algorithm. Implementation of the proposed method is discussed in section III. Performance evaluation and result discussion are given in section IV. Finally, section V provides some comments regarding the conclusion.

2. Inrush current phenomenon

Magnetization inrush current is a well-known phenomenon in the power transformers and due to the large magnitude and non-sinusoidal waveform, it may have significant consequences on the voltage drop of the grid, mal-operation of protective relays, and motor vibration. During the normal operation of a power transformer, the core linkage flux (λ_m) remains in the linear region and below the saturation flux (λ_k). But when a transformer is energized, the core linkage flux (λ_m) may enhance beyond the saturation level (λ_k). In the following the inrush phenomenon is mathematically analyzed. Fig. 1 illustrates a typical power transformer that is connected to a power grid. The equivalent circuit of Fig. 1 after transformer switching is provided in Fig. 2.

As it can be seen in Fig. 2, R and L show the winding resistance and leakage inductance of the primary side of the transformer respectively. Note that the transformer is assumed at no-load condition during inrush current analysis. It is assumed the voltage of power grid is expressed as follows:

$$v(t) = V_1 sin(\omega t + \theta_0) \tag{1}$$

Based on the notations illustrated in Fig. 2, the instantaneous flux ($\lambda(t)$) is the sum of core linkage flux (λ_m) and leakage flux (λ_l). The instantaneous flux ($\lambda(t)$) is calculated as follows:

$$\begin{aligned}\lambda(t) &= \lambda_m(t) + \lambda_l \\ &= \int_0^t (v(t) - Ri(t))dt + \lambda_r \\ &= -\frac{V_1}{\omega}cos(\omega t + \theta_0) + \frac{V_1}{\omega}cos(\theta_0) + \lambda_r - \int_0^t Ri(t)dt\end{aligned} \tag{2}$$

To conduct analysis on the terms of instantaneous flux ($\lambda(t)$), expression (2) is represented as follows:

$$\lambda(t) = \lambda_v(t) + \lambda_0 - \lambda_{Ri}(t) \tag{3}$$

where:

$$\lambda_v(t) = -\frac{V_1}{\omega}cos(\omega t + \theta_0) = -\lambda_1 cos(\omega t + \theta_0) \tag{4}$$

$$\lambda_0 = \frac{V_1}{\omega}cos(\theta_0) + \lambda_r \tag{5}$$

$$\lambda_{v0} = \frac{V_1}{\omega}cos(\theta_0) = \lambda_1 cos(\theta_0) \tag{6}$$

$$\lambda_{Ri}(t) = \int_0^t Ri(t)dt \tag{7}$$

From expression (5) it can be concluded that the DC residual flux linkage (λ_r) is an influential factor in driving the transformer to saturation region. After transformer de-energization, while the transformer magnetization voltage and current become zero, due to the core's hysteresis loop behavior, the flux may not become zero and the certain remnant DC flux may remain in the transformer's core. Therefore, after the next energization, the remnant DC flux will be added to the instantaneous flux developed by the grid applied voltage. It should be noted that due to the polarity of the remnant DC flux, it can impose positive or negative impact on driving the transformer to the saturation.

According to expression (6), DC flux due to transformer energization (λ_{v0}) can vary between $-\lambda_1$ and $+\lambda_1$, depending on the switching angle

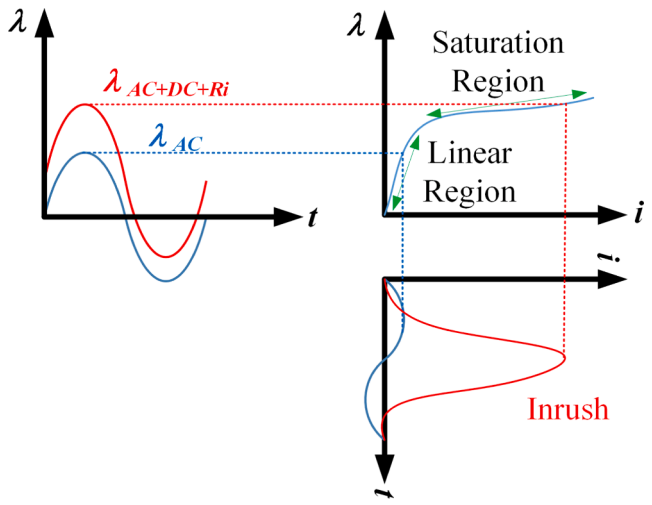

Fig. 3. Behavior of power transformer in linear and saturation region of excitation curve.

(θ_0). Note that λ_1 is the steady state value of linkage flux. It should be noted that DC flux due to transformer energization (λ_{v0}) can be generally produced after any sudden voltage changes. Overall, from expression (5), DC flux of the transformer (λ_0) contains λr and λ_{v0} and it can enter the transformer into the saturation region, and consequently causes inrush current.

Expression (7) shows the lost-flux ($\lambda_{Ri(t)}$) due to the integral of voltage drop ($Ri(t)$). This term can be also considered as an influential term on amplifying the probability of transformer saturation and consequently inrush current phenomenon.

From above-mentioned discussion it is concluded that due to non-linear behavior of the power transformer, the inrush current has not only a large magnitude but also non-sinusoidal waveform. The behavior of the power transformer in the linear and non-linear regions are shown in Fig. 3.

However, during faults and due to voltage drop, the power transformer operating point goes in the linear region and as a result, the current waveform during fault remains almost always sinusoidal [28]. Note that CT also has the same behavior as shown in Fig. 3. The difference between CT and a power transformer is that the CT is connected in series in the power system and it behaves in the linear region for a large amount of current. Nevertheless, due to flux asymmetry, the CT's primary current may drive CT to saturation region. The CT saturation which may be usually seen during fault condition, makes the current waveform distorted and non-sinusoidal. Obviously it is mandatory to detect internal fault conditions even during CT saturation.

The aim of this paper is to find an efficient way to enhance the immunity of the transformer's differential protection against mal-operation during transformer energization. As a result, in the following, an algorithm is proposed that it distinguishes the internal fault currents from external fault or inrush currents based on the distance of the phase angles of the CT's currents. During internal fault condition, during the internal fault, the phase angles of the current signals of CTs are in phase. As a result, the distance of the phase angles during internal fault conditions is very low. However, during the external fault, the phase angles of the current signals of CTs are 180° out of phase. Also, during inrush current, the phase angle does not fit on a sinusoidal waveform and it has significant variations. As a result, in both inrush or external fault conditions, the distance between phase angles of CT's currents are very significant. Therefore, in this paper, such a distance is utilized to distinguish the internal fault currents from external fault or inrush currents.

3. Proposed algorithm

As mentioned, the proposed method is based on measuring the distance between the phase angles of the CT's current signals. As a result, it is essential to estimate the phase angle from the current signals. During fault, the fault current signal is expressed as follows:

$$i(t) = I_m cos(\omega t + \theta) + I_{dc} e^{-t/\tau} \tag{8}$$

where I_m and I_{dc} show the magnitude of the fundamental component and the decaying DC offset component respectively. Also ω, θ and τ denote the frequency, phase angle, and time constant, respectively. While the proposed index is based on the phase angle (θ), it is mandatory to deal with the oscillations of the decaying DC term on the phase angle (θ).

To obtain the phase angle, two calculation procedures are combined: at first, an estimation of the decaying DC time constant is calculated. Afterwards, the estimated time constant will be utilized to modify the recursive least squares (RLS) technique formulation so that the unwanted oscillations due to the decaying DC term will be removed from the estimated phase angle. In the following first the time constant of DC term is estimated and then modified RLS based formulation for phase angle estimation is described.

A. Calculating time constant

It has been acknowledged that the DC component has a significant impact on phasor estimation [1,28]. As a result, a DC removal filter should be used in combination with the phasor estimation algorithm to remove the inaccuracy due to the DC component in the phase angle estimation [1,28].

To remove the impact of the decaying DC term, here, a formulation based on the derivation is presented that estimates the time constant. Assuming D as the derivation operator, the first (D), second (D^2), and third (D^3) derivations of the fault current signal expressed by (8), is calculated as follows:

$$Di(t) = -(\omega) I_m sin(\omega t + \theta) - \frac{I_{dc}}{\tau} e^{-t/\tau} \tag{9}$$

$$D^2 i(t) = -(\omega)^2 I_m cos(\omega t + \theta) + \frac{I_{dc}}{\tau^2} e^{-t/\tau} \tag{10}$$

$$D^3 i(t) = (\omega)^3 I_m sin(\omega t + \theta) - \frac{I_{dc}}{\tau^3} e^{-t/\tau} \tag{11}$$

Having the derivations of the fault current in expressions (9) to (11), the time constant is calculated according to the following expression:

$$\frac{D^2 i(t) + (\omega)^2 i(t)}{D^3 i(t) + (\omega)^2 Di(t)} = \frac{-\frac{I_{dc}}{\tau^2} e^{-t/\tau} - (\omega)^2 I_{dc} e^{-t/\tau}}{-\frac{I_{dc}}{\tau^3} e^{-t/\tau} - (\omega)^2 \frac{I_{dc}}{\tau} e^{-t/\tau}} = \tau \tag{12}$$

By estimating the time constant using expression (12), the RLS can be formulated so that it removes the impact of the decaying DC component from the phase angle. In the next section, the formulations of the RLS technique are described.

B. Calculating phase angle

To calculate the phase angle of the fault current, first it is mandatory to identify the matrices of known components and unknown parameters. Since in practice, the signal is discretely fed to the relay, it is proper to formulate the parameter estimation in discrete form. To such aim, the mathematical model of the current signal during a fault, $\hat{i}$, can be expressed in discretized form as follows:

$$\begin{aligned} \hat{i}(k) &= I_m cos(\theta) cos(\omega k \Delta t) \\ &- I_m sin(\theta) sin(\omega k \Delta t) + I_{dc} e^{-k\Delta t/\tau} \end{aligned} \tag{13}$$

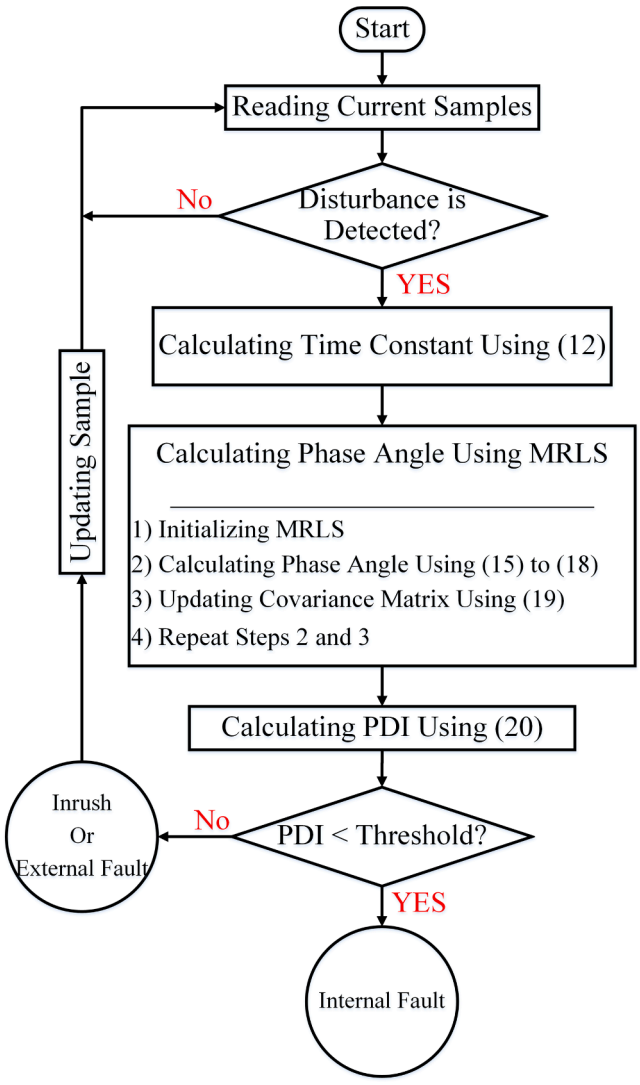

Fig. 4. Proposed algorithm implementation procedure.

where $\widehat{i}(k)$ is the *k-th* sample of the fault current. Also, Δt denotes the sampling time interval. Rewriting (13) in a compact form, the following can be concluded:

$$\widehat{i}(k) = \Gamma_x \mathrm{I}_x + e(k) \tag{14}$$

where, Γ_x and I_x are the matrices of known components and unknown parameters, respectively, and are defined as follows:

$$\mathrm{I}_x = \begin{bmatrix} I_m cos(\theta) & -I_m sin(\theta) & I_{dc} \end{bmatrix}^T \tag{15}$$

$$\Gamma_x = \begin{bmatrix} cos(\omega k \Delta t) & sin(\omega k \Delta t) & e^{-k\Delta t/\tau} \end{bmatrix} \tag{16}$$

To find the unknown parameters from (16), RLS technique provides the following solution:

$$\widehat{\mathrm{I}}_x(k+1) = \widehat{\mathrm{I}}_x(k) + \Psi(k+1)e(k+1) \tag{17}$$

where Ψ is the gain matrix and is expressed as follows:

$$\Psi(k) = \mathrm{P}(k)\mathrm{I}_x(k) \tag{18}$$

In (18), P denotes the covariance matrix and is updated in each time step of the phasor estimation. Several methods have been introduced for updating the covariance matrix to preserve the adaptive nature of the RLS algorithm including the forgetting factor method, covariance resetting, random walking, and hybrid algorithms [29]. While discussing the performance of these algorithms is not the intention of this paper, a hybrid algorithm for updating the covariance matrix which is suggested in [29], is utilized as follows:

$$\mathrm{P}(k+1) = \begin{cases} \mathrm{P}(k) - \dfrac{\mathrm{P}(k)\Gamma_x(k)\Gamma_x^T(k)\mathrm{P}(k)}{1+\Gamma_x^T(k)\mathrm{P}(k)\Gamma_x(k)} & |e(k)| \le \xi \\ \mathrm{P}(k) + \mathrm{X} & |e(k)| \ge \xi \end{cases} \tag{19}$$

where X is a positive diagonal matrix that avoids the covariance matrix trance from reaching reduced value before the convergence of the parameters. X can be contained by zero mean random variables or constant values. Here X is defined by $\sigma^2\mathbf{I}$ in which, $\mathbf{I}$ is the identity matrix and σ^2 is the covariance parameter. By increasing the covariance σ^2, the gain and consequently the convergence speed, is also increased and the results of the estimation become less reliable. On the contrary, by decreasing σ^2, the speed of convergence is decreased. According [29], σ^2 is selected 0.1.

Moreover ξ helps to avoid the covariance matrix reaching the reduced values before the final convergence. In other words, it keeps the updating covariance matrix given in (19) activated all the time. Note that the expression (19) only stops after the convergence has been achieved. Also, ξ is an arbitrary threshold and is selected 0.1 which is obtained by trial and error.

C. Proposed index

The proposed method distinguishes the internal fault currents from external fault or inrush currents based on the distance of the phase angles of the CT's currents. During internal fault condition, during the internal fault, the phase angles of the current signals of CTs are in phase. However, during the external fault, the phase angles of the current signals of CTs are 180° out of phase. Besides, during the inrush phenomenon, the phase angle does not fit on a sinusoidal waveform and it has significant variations. As a result, in both inrush or external fault conditions, the distance between phase angles of CT's currents are very significant. Proposed index is designed based on the latter-mentioned distance to distinguish the internal fault currents from external fault or inrush currents. The distance between phase angles is calculated using normalized mean residue (NMR). NMR is a well-known effective tool in information theory for determining the variance between a pair of objects in a dataset [30]. NMR removes the similarity between a pair of objects in a dataset ensuring the noise insensitivity in the data. It is assumed that Θ_{CT1} and Θ_{CT2} are the two vectors of the estimated angles of the CT's current signals. As a result, the proposed discrimination index (PDI) based on the NMR is introduced as follows:

$$PDI(\Theta_{CT1}, \Theta_{CT2}) = \frac{\sum_{i=1}^{n} \left| (\theta_{CT1,i} - \theta_{CT1,i}^{lm}) - (\theta_{CT2,i} - \theta_{CT2,i}^{lm}) \right|^2}{max(\sum_{i=1}^{n} \left| \theta_{CT1,i} - \theta_{CT1,i}^{lm} \right|^2, \sum_{i=1}^{n} \left| \theta_{CT2,i} - \theta_{CT2,i}^{lm} \right|^2)} \tag{20}$$

where $\theta_{CT1,i}$ and $\theta_{CT2,i}$ are the fundamental phase angles belong to CT1 and CT2 respectively. Also *lm* denotes the local mean and it is calculated as follows:

$$if \quad i = 1, \qquad \theta_{CT,i}^{lm} = \frac{\theta_{CT,i} + \theta_{CT,i+1}}{2}$$

$$if \quad 1 < i < n, \quad \theta_{CT,i}^{lm} = \frac{\theta_{CT,i-1} + 2\theta_{CT,i} + \theta_{CT,i+1}}{4}$$

$$if \quad i = n, \qquad \theta_{CT,i}^{lm} = \frac{\theta_{CT,i-1} + \theta_{CT,i}}{2}$$

Expression (20) simply measures between the phase angles of the CT's currents. As it can be seen in (20), the local mean is calculated by 2 points for the first and last data, and by 3 points for the other samples of data. As a result, it can quickly measure the distance between the phase angles.

Table 1
Specification of the influential variables.

Variable	Distribution Function	Range
Switching Instance	Continuous Uniform	[0-360°]
Fault Resistance	Continuous Uniform	[0–5 Ω]
Fault Inception Angle	Continuous Uniform	[0-360°]
Fault Type	Continuous Uniform k ∈ [0–1]	k ∈ [0–0.75]: Single Phase to Ground k ∈ [0.76–0.85]: Double Phase k ∈ [0.86–0.95]: Double Phase to Ground k ∈ [0.96–1]: Three Phase to Ground
Remnant Flux	Continuous Uniform	[-40%-40%]
Noise Level	Continuous Uniform	[30 dB- 60 dB]

Table 2
The Values of PDI in different conditions (In first quarter of cycle after disturbance).

Condition	Minimum	Maximum
Internal Fault (with/without CT saturation)	0.05	0.23
Simultaneously Inrush and Internal Fault	0.08	0.25
External Fault (with/without CT saturation)	0.66	0.98
Inrush	0.47	0.97

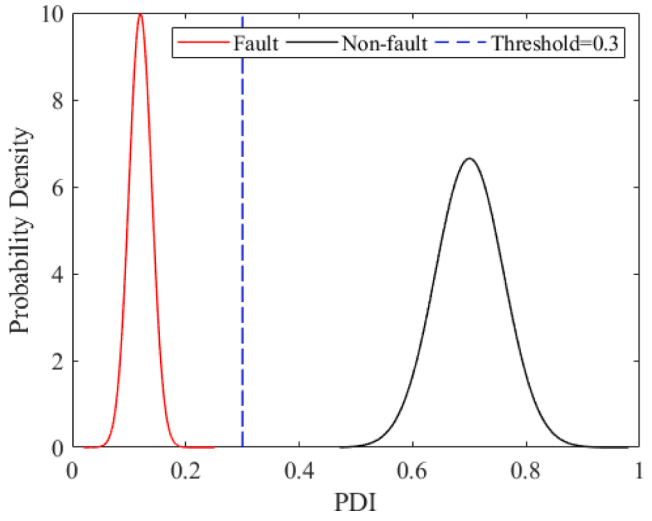

Fig. 5. PDFs for the PDI and the selected threshold.

4. Implementation procedure

The proposed algorithm implementation is shown in Fig. 4. The following procedure is performed for discrimination of the internal faults and inrush currents:

1) Reading current samples: The samples are acquired with a rate of 100 samples/cycle. As a result, the step time for 50 Hz is 200 microseconds. Using the sampled currents of CTs, the operating current ($I_{Op} = \left|\vec{I}_{CT,1} + \vec{I}_{CT,2}\right|$) is calculated and if it triggers the relay's operating setting, then the signals of both CTs will be fed to the algorithm. As a result, the disturbance is detected if the operating current triggers the relay's operating setting. In this investigation, the disturbance is identified if the operating current becomes greater than 10% of the nominal current.
2) Calculating the fundamental phase angle: Utilizing a sliding window with 10 samples, the current samples of the sub-cycle sliding window are fed to (14) to (18) to calculate the fundamental phase angle. Note that after the estimation of the time constant using (12), the matrix of known components Γ_x is calculated. Afterward, within the given window, the unknown parameters I_x are calculated. In each iteration of the calculation, the covariance matrix is updated using (19). Note that the above procedure is repeated once the sliding window is updated.
3) Calculating PDI: The estimated fundamental phase angles are fed to (20) to calculate the distance between the phase angles.
4) Decision making: Eventually, the PDI is compared with a certain threshold to identify the internal faults. PDI identifies an internal fault when it remains below the threshold for 5 consecutive sliding windows. Also, for inrush and external fault conditions, the decision is made when PDI crosses the threshold for 5 consecutive sliding windows. It should be noted that the sliding window has 10 samples and updates sample by sample.

5. Validation of proposed index

Here, the performance of the proposed discrimination index is evaluated with several simulations and experimentally recorded data.

A. Selecting threshold

To obtain a threshold, plenty of simulations are conducted according to several influential parameters given in Table 1. The simulations were conducted for more than 3000 simulated scenarios considering several influential parameters given in Table 1 including switching instances with a range between [0-360°], fault resistance with a range between [0–5 Ω], fault inception angle with a range between [0-360°], noise level with a range between [30 dB-60 dB], remnant flux [-40%- 40%], and different types of short circuit faults. The parameters are considered as random variables and in each simulation they were randomly changed based on the distribution function and corresponding range given in Table 1.

As shown in Table 2, through a sensitivity analysis described in the previous paragraph, the minimum and maximum values for PDI in different conditions are obtained. Note that the values of PDI are obtained in the first quarter of the cycle.

The results of the Tables 2 were obtained for more than 3000 simulated scenarios considering several influential parameters given in Table 1. The simulated scenarios include 1739 scenarios for internal fault with/without CT saturation, 100 scenarios for simultaneously internal fault with inrush current, 1137 scenarios for inrush current with/without remnant flux, and 250 scenarios for external fault with/without CT saturation. To determine the threshold, Otsu thresholding method is employed in the following [31]. Otsu thresholding method is implemented in three general steps as follows:

First step: Finding Probability Function Density (PDF) for the desired parameter (PDI) considering different fault and non-fault conditions. According to Table 1, the fault and non-fault conditions are grouped as follows:

- Fault condition which includes internal fault (with/without CT saturation) and simultaneously inrush and internal fault.
- Non-fault condition which includes inrush and external fault (with/without CT saturation).

Second step: Fitting a normal function PDF for each case (fault and non-fault conditions).

Third step: Finding the intersection point of the two PDF curves. The intersection is considered as the threshold value.

Table 3
The behavior of the RLS for different covariance parameter.

	Accuracy (%)	Average Reponses Time (ms)
$\sigma^2 = 0.01$	15.8	1.1
$\sigma^2 = 0.05$	7.1	2.4
$\sigma^2 = 0.1$	1.7	3.9
$\sigma^2 = 0.2$	1.1	9.8
$\sigma^2 = 0.5$	0.6	24
$\sigma^2 = 0.9$	0.1	39

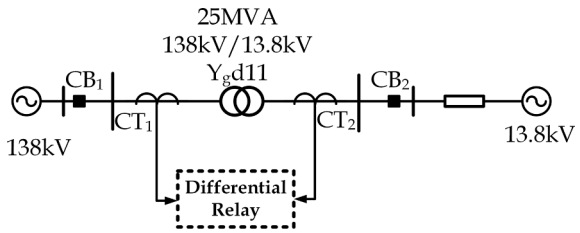

Fig. 6. Power transformer for simulation in MATLAB environment.

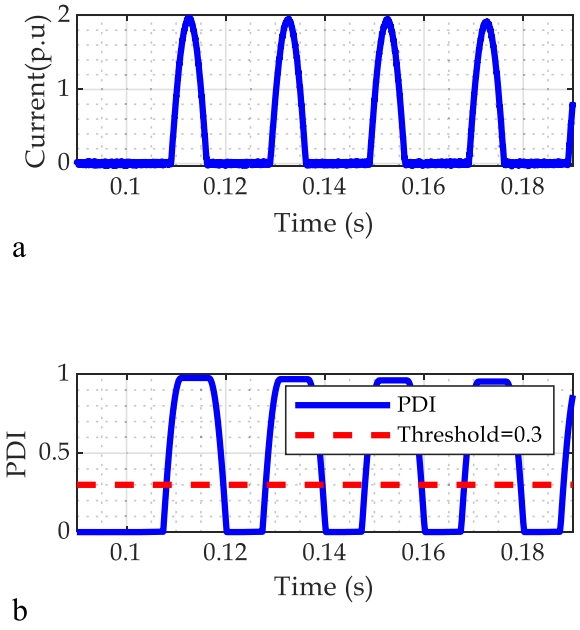

Fig. 7. Performance of the proposed algorithm for inrush current, (a) inrush current signal with 30 dB noise, (b) proposed index.

As illustrated in Fig. 5, the PDFs have no intersection and as a result, the obtained threshold can clearly discriminate the internal fault and inrush current scenarios.

It should also be noted that while the threshold is calculated based on several fault and inrush conditions from simulation and experimental data, it only depends on the waveform deformation from the standard fault signal (8) and has no dependency on the power transformer parameters.

The initial condition of RLS is obtained through applying several test simulation cases. In general, the covariance matrix P that needs to be initialized. This matrix is initialized by the covariance parameter σ^2. To find optimum covariance parameters, 1989 internal and external fault scenarios are applied to the RLS algorithm. The obtained phase angle using RLS algorithm was compared with full-cycle discrete Fourier transform (DFT) as the reference. The error of estimation was calculated as follows:

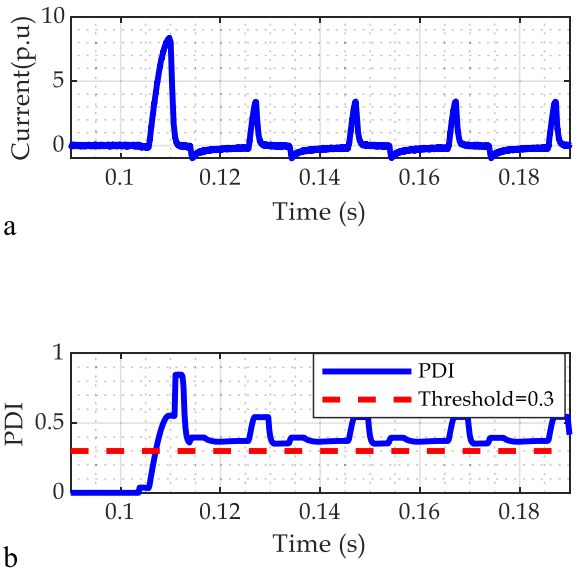

Fig. 8. Performance of the proposed algorithm for inrush current energizing with residual flux with 30 dB noise, (a) inrush current signal, (b) proposed index.

$$Error\% = \left|\frac{\theta_{RLS} - \theta_{DFT}}{\theta_{DFT}}\right| \times 100 \tag{21}$$

The average of accuracy for different values of covariance parameters are obtained and tabulated in Table C. As it can be seen in Table 3, by increasing the covariance parameter, both accuracy and response time of the estimation are enhanced. Since the proposed method requires to deal with CT saturation conditions it should be able to estimate phase angle in less than a quarter of a cycle to be able to deal with deep saturation. As a result, the covariance parameter σ^2 is selected 0.1.

B. Simulation results

To obtain the internal fault and inrush current scenarios from the simulation environment, a Y_gd11, 138/13.8 kV transformer which is shown in Fig. 6 is selected for simulation in the MATLAB environment. The phase displacement due to the vector group will result in differential protection' mal-operation. The transformer of interest in this paper has a vector group Ygd11 which means the LV winding leads the HV winding by 30°. To compensate for the latter phase displacement, phase compensation is performed by means of wiring current transformers either delta or wye.

The requirements for the implementation of the test system consist of Thevenin impedances, transformer characteristics, and characteristics of CTs, are provided in appendix. More than 3000 scenarios are applied to the proposed algorithm including different internal fault scenarios with/without CT saturation, inrush current, and inrush current with internal fault. During the acquisition of the simulated scenarios, various variables are taken into consideration, which are listed in Table 1.

1) Inrush

Energizing the power transformer at t = 0.105 s, an inrush signal is produced and fed to the proposed index. As one can see in Fig. 7b, after about 3 ms of the transformer switching the PDI varies and exceeds the threshold.

Energizing the power transformer with 60% residual flux at t = 0.104 s, an inrush current is generated. As it is obvious in Fig. 8b, the SHR algorithm identifies the inrush current in less than a quarter of a cycle.

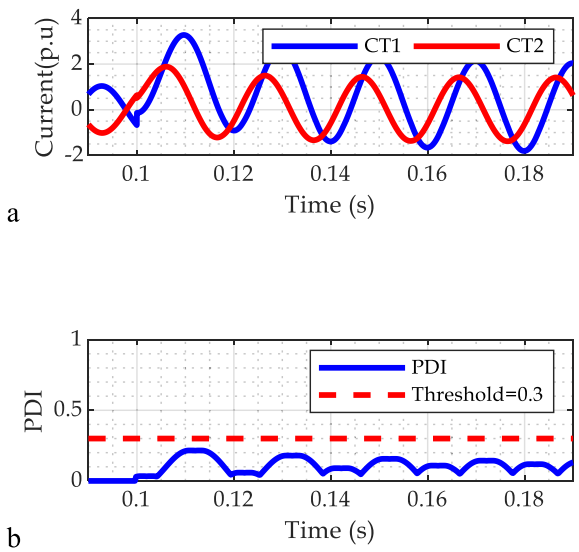

Fig. 9. Performance of the proposed algorithm for simulated internal fault without saturation, (a) fault current signals, (b) proposed index.

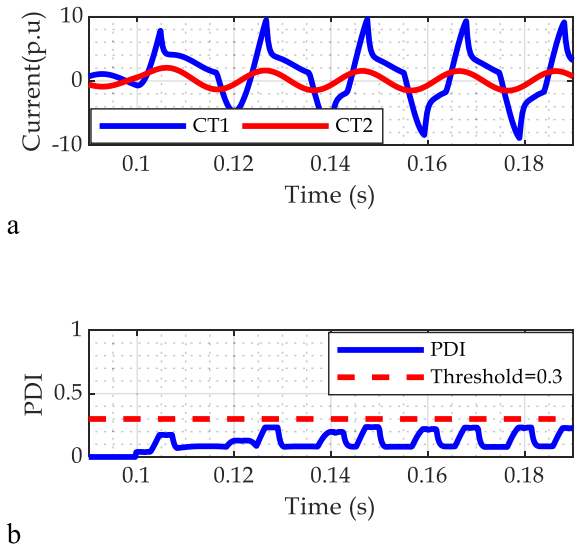

Fig. 10. Performance of the proposed algorithm for internal fault with CT saturation, (a) fault current signal, (b) proposed index.

From Figs. 7 and 8, it can be seen that the PDI quickly changes due to the fact that the inrush current does not fit on a standard fault signal (8) and as a result, the phase angle of the inrush current and consequently the PDI start to varying in time.

2) Internal fault

Applying an internal fault on 15% of the star side of the power transformer winding at t = 0.1 s, an internal fault scenario is produced as shown in Fig. 9a. As it can be observed in Fig. 9b, the PDI remains below the threshold after disturbance which means the internal fault is identified.

Much more challenging scenarios can happen during CT saturation, where the current signal contains distortions and thus the differential protection may mal-operate in discrimination between fault and inrush scenarios. Such a signal which is provided in Fig. 10a, and applied to the methods. As shown in Fig. 10b, due to the employment of the data for the un-saturated region, the proposed algorithm is successfully able to recognize the internal faults.

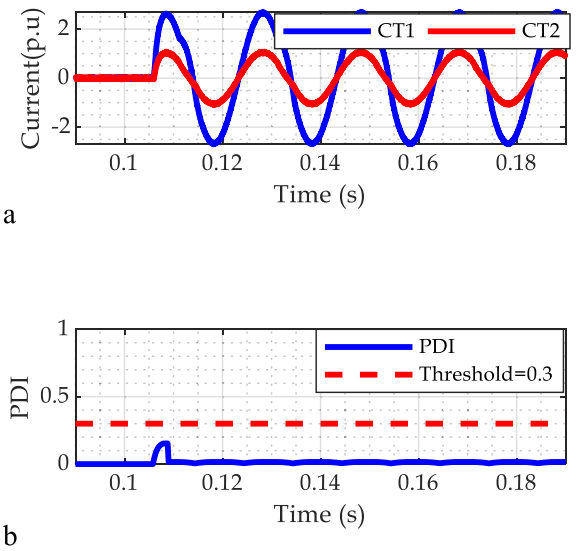

Fig. 11. Performance of the proposed algorithm for transformer energization with internal fault with 50 dB noise, (a) internal fault current during transformer energization, (b) proposed index.

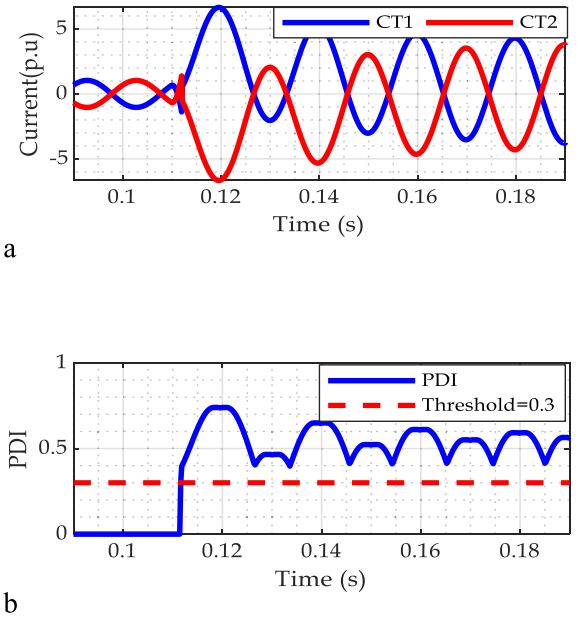

Fig. 12. Performance of the proposed algorithm for external fault, (a) fault current signal, (b) proposed index.

In both cases of internal fault given in Figs. 9 and 10, due to the minor variations of the phase angle the PDI does not cross the threshold. As a result, the PDI is able to identify the internal fault even in the case of CT saturation.

3) Transformer energization with internal fault

Considering an internal fault during transformer energization, the differential relays may mal-operate in this condition. To simulate such a circumstance, a 25% fault in the star side of the power transformer is applied at t = 0.106 s and resultant signals are further fed to the methods as shown in Fig. 11. As illustrated in Fig. 11.b, the proposed method can identify such an internal fault. During transformer energization with an internal fault, the faulty phase has a similar current waveform to the (8).

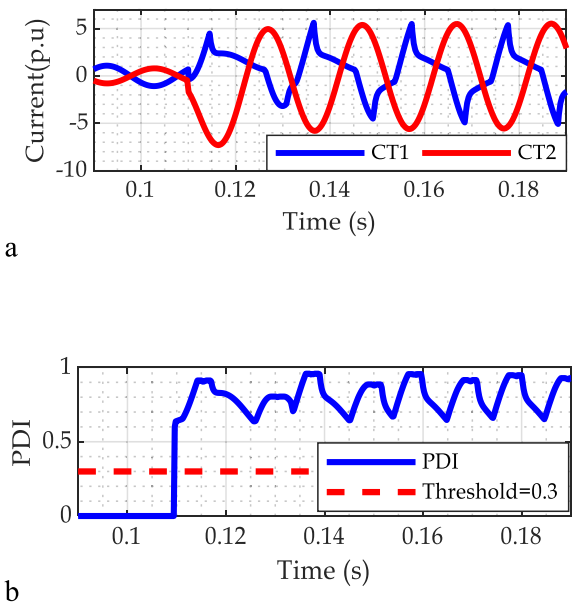

Fig. 13. Performance of the proposed algorithm for external fault with CT saturation, (a) fault current signal, (b) proposed index.

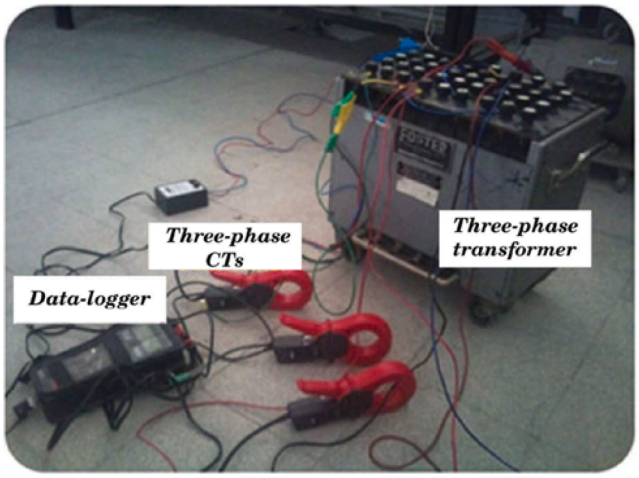

Fig. 14. Experimental Setup for Performance Evaluation of the Proposed Method.

As a result, during such a disturbance, the phase angle variations and consequently the PDI are much lower than the threshold.

4) External fault

Applying a fault on phase A near CB2 in Fig. 2 at t = 0.112 s, an external fault scenario is produced as shown in Fig. 12a. Fig. 12b illustrates that the PDI crosses the threshold almost 3.5 ms after disturbance. As a result, the signal is not identified as an internal fault.

The knee point of CTs are designed to operate in the linear zone for short circuit currents less than 10 times of nominal current. However, to create the saturation, extra resistance is added to the burden of CT1 (CT at the high voltage side of the power transformer) to create a saturation condition. As it can be seen in Fig. 13, during an external fault accompanied by CT saturation, where the current signal contains distortions, the PDI successfully discriminates the non-internal fault condition. In both cases of internal fault given in Figs. 12 and 13, due to significant variation of the phase angle, the PDI crosses the threshold almost after 4 ms. As a result, the PDI does not operate during external faults even in the case of CT saturation.

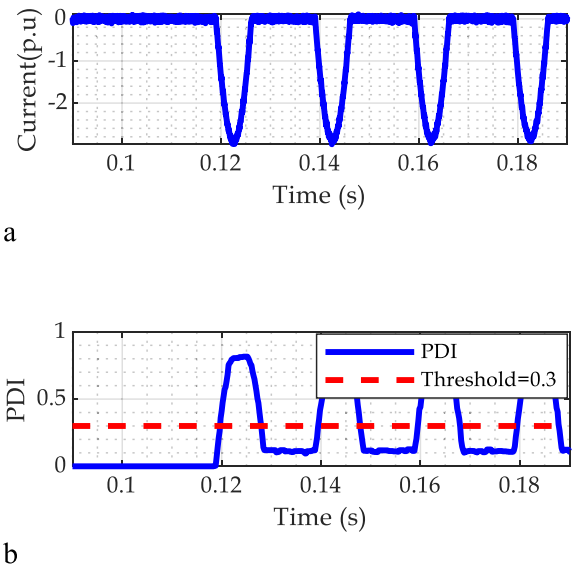

Fig. 15. Performance of the proposed algorithm for inrush current, (a) inrush current signal, (b) proposed index.

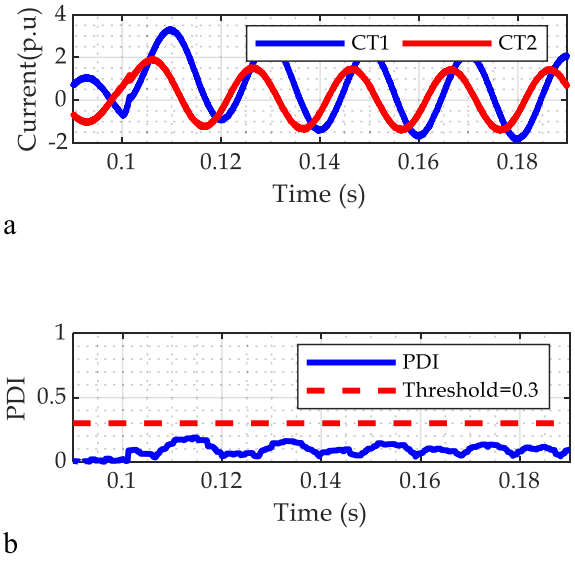

Fig. 16. Performance of the proposed algorithm under experimental internal fault condition, (a) fault current signals, (b) proposed index.

C. Performance validation using experimental recorded signals

The experimental setup which is shown in Fig. 14 is provided to generate some experimental fault and inrush current signals. The experimental setup contains a power transformer with 6 KVA nominal apparent power. The power transformer operates at 50 Hz, with the voltage level of 330/330 V. The power transformer has different access terminals of the windings for recording internal faults. Several inrush and fault signals are generated and recorded considering 128 microseconds sampling time for the data logger.

According to Fig. 15, the PDI index is able to identify the inrush current in almost 3 ms after transformer energization. In the case of internal fault shown in Fig. 16, the PDI has low value due to low variation of phase angle of currents. On the contrary, as shown in Fig. 17, in the case of external fault, the PDI has large value due to the phase

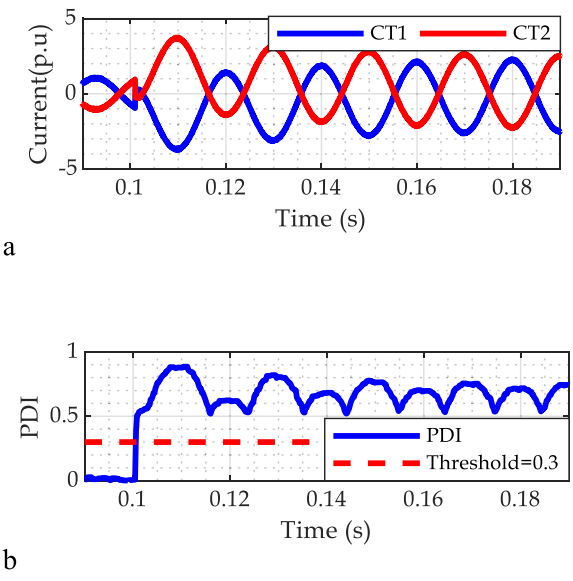

Fig. 17. Performance of the proposed algorithm for recorded external fault condition, (a) fault current signals, (b) proposed index.

Table 4
Comparison References [23–25,27] and the proposed algorithm.

	[23]	[24]	[25]	[27]	PDI
Requiring An extra index for CT saturation detection	No	No	No	Yes	No
Immune operation during CT saturation	Yes- with delay	Yes- with delay	Yes	Yes	Yes
Considering decaying DC During Fault in Formulation	No	No	No	Yes	Yes
Required ideal data from current signal	1 Cycle	< ½ cycle	1 Cycle	¼ cycle	¼ cycle
Average operating time during different scenario	<1 cycle	< ½ cycle	<¼ cycle	< ½ cycle	< ¼ cycle
Complexity	Medium	Medium	Low	High	Medium

Table 5
Statistical data of the performance of the proposed index and state-of-the-art algorithms for 1137 inrush scenarios.

	[23]	[24]	[25]	[27]	PDI
Minimum (ms)	18.15	11.02	4.25	3.86	3.35
Maximum (ms)	21.13	13.64	5.08	5.41	4.29
Average (ms)	19.02	11.61	4.67	4.04	3.85
% of Correct Identification	95	96	100	100	100

Table 6
Statistical data of the performance of the proposed index and state-of-the-art algorithms for 1793 internal fault scenarios.

	[23]	[24]	[25]	[27]	PDI
Minimum (ms)	20.31	10.26	4.57	4.86	3.21
Maximum (ms)	28.13	14.4	19.8	11.41	4.69
Average (ms)	23.21	13.61	10.71	5.04	4.25
% of Correct Identification	96	95	99	99	100

content of the current signals. In general, the proposed method requires only 3 to 4 ms of data for reaching a reliable decision. Eventually, the results indicate that the PDI has noise sensitivity.

Table 7
Statistical data of the performance of the proposed index and state-of-the-art algorithms for 100 scenarios of transformer energization with internal fault.

	[23]	[24]	[25]	[27]	PDI
Minimum (ms)	17.59	10.97	3.98	4.25	3.33
Maximum (ms)	25.67	15.12	12.42	5.1	4.12
Average (ms)	22.76	11.79	7.58	4.51	3.63
% of Correct Identification	89	92	94	95	99

Table 8
The comparison between RLS and Kalman filter (the results are in percentage).

	$\tau = 10$ ms		$\tau = 50$ ms		$\tau = 100$ ms	
	RLS	Kalman	RLS	Kalman	RLS	Kalman
$\theta = 0°$	1.8	2.1	1.9	1.8	2.1	2
$\theta = 30°$	2.1	1.4	2.4	1.9	3.2	2.5
$\theta = 60°$	1.7	1.9	2.3	1.7	2.7	1.9
$\theta = 90°$	2.4	2.8	1.5	1.8	1.9	1.6
$\theta = 120°$	1.6	2.1	1.6	2.4	2.8	1.5
$\theta = 150°$	2.6	2.4	1.9	2.3	1.7	2.4
$\theta = 180°$	2.3	1.8	1.6	2	2.9	2.7

Table 9
The comparison between RLS and Kalman filter for internal fault scenarios with/without CT (the results are in percentage).

	Without CT saturation		With CT saturation	
	RLS	Kalman	RLS	Kalman
Accuracy (%)	100	100	100	100
Average Response Time (ms)	3.85	4.1	4.12	4.89

Table 10
The specification of the test system.

Component	Specifications
138 kV source	R_+=7.1 Ω, L_+=53.99mH R_0 = 7.596 Ω, L_0 = 115.45mH
13.8 kV source	R_+=1.4 Ω, L_+=5.6mH R_0 = 1.498 Ω, L_0 = 11.957mH
Power transformer	R_1 = 0.908 Ω, L_1 = 78.51mH R_2 = 0.0091 Ω, L_2 = 0.7851mH R_c = 1.19MΩ,
Transmission line	R_1 = 0.3101 Ω, L_1 = 2.41mH C_1 = 26.8nF, R_0 = 0.1437 Ω L_0 = 11.45mH, C_0 = 5.635nF

Table 11
Specification of the CTs.

	Turn Ratio	Mean core length	Cross section area	Winding resistance	Burden
CT1	100	42.5 cm	30 mm^2	2.3 Ω	10 VA
CT2	1200	106 cm	97 mm^2	7.2 Ω	20 VA

D. Comparison proposed method with other algorithms

In this section performance comparison of the proposed method with the related recent algorithms is provided. Table 4 shows the qualitative comparisons between the proposed method and the methods in Refs. [23–25] to [27]. From Table 4, it is observed that:

- Except Ref. [27], the other methods do not need extra criterion for CT saturation detection. Besides, all algorithms show good performance during CT saturation and the differences are in the time delays.

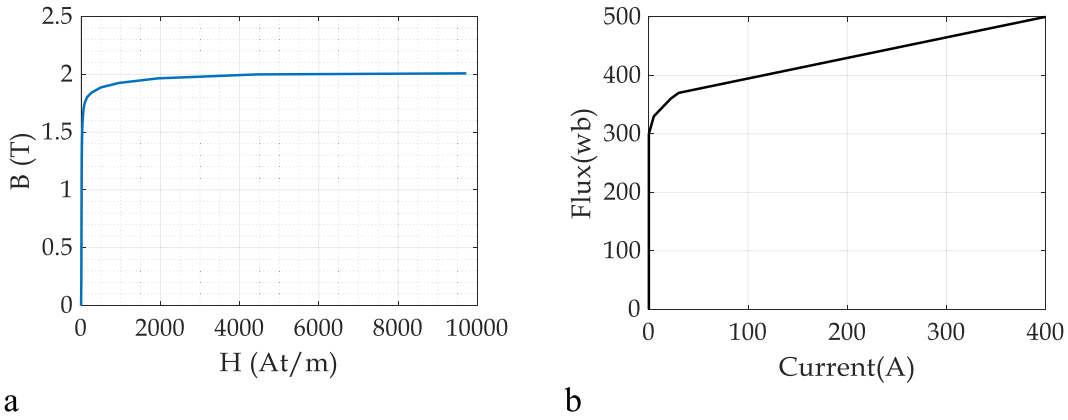

Fig. 18. (a) Magnetization Curve of CTs, (b) Magnetization Curve of Transformer.

- Refs. [23–25] do not mathematically eliminate the decaying DC component, while both Ref. [27] and the proposed method remove the impact decaying DC component from proposed indices.
- Refs. [23] and [24] need one cycle and half cycle data for executing their calculation respectively. Also, Ref. [25] needs one cycle current signal for normalizing current signal. However, both Refs. [25] and [27] utilize a quarter cycle to calculate its index. On the contrary, the proposed index needs a sub-cycle data of current signal to calculate the proposed index.
- For Ref. [23], the average operation time (AOT) during different scenarios is less than one cycle. The AOT for Refs. [24,27] are less than half cycle and for Ref. [25] and proposed method, are less than quarter of cycle respectively. In comparison with the previous point, the PDI has supremacy both in requiring lowest data and response time compared with the other methods.
- Eventually, while the Ref. [25] has lowest complexity, but taking into account all of the challenges given in Table 4, it is observed that the proposed index has more flexibility and reliability in discrimination of internal fault and inrush current with and fast response.

Tables 5 to 7 shows the quantitative comparisons between the proposed method and the methods in Refs. [23–25] to [27].

- From Table 5, it is observed that PID has the fastest response with high accuracy in the identification of inrush currents.
- From Table 6 shows the PID identifies the fault currents in less than a quarter of a cycle with promising accuracy. Fast parameter estimation within the un-saturated interval considering the impact of the decaying DC has made the proposed algorithm more immune to CT saturation compared with other methods.
- Eventually, according to Table 7 in the case of internal fault during transformer energization, the PDI has the highest response and precision in comparison with other algorithms.

Overall, Tables 4 to 7 indicate that the proposed method is able to discriminate the internal fault from inrush currents considering different challenging scenarios.

E. Performance comparison proposed index using different phasor estimators

This section is dedicated to performance comparison of the proposed index using different phasor estimators. To achieve this aim, the Kalman filter is selected as the fast sub-cycle estimator to implement the PDI. The process of the Kalman Filter is very similar to the recursive least squares. While recursive least squares update the estimate of a static parameter, Kalman filter is able to update and estimate of an evolving state. Note that RLS with forgetting factor can be employed for slow time-varying signals.

Besides, from complexity of the implementation, the standard RLS has complexity of $O(N^2)$. Of course with some modifications, the complexity can be reduced to $O(N)$. On the contrary, the standard Kalman filter has complexity of $O(N^3)$ and with some modifications can be reduced to $O(N^2)$ [32].

To show the accuracy of the RLS and Kalman filter in the phase angle estimation, a test signal with the following condition is provided:

$$i(t) = I_m cos(\omega t + \theta) + I_{dc} e^{-t/\tau} \tag{22}$$

where $I_m = 10$ (p.u) $I_{dc} = 10$ (p.u), Also $\omega = 100\pi$. For the evaluation, the time constant (τ) and the phase angle (θ) are changed and the accuracy of the estimated phase angle is compared with actual value. The error of the estimation is provided in Table 8. The inaccuracy of the estimation is calculated as follows:

$$Error\% = \left| \frac{\theta_{Estimated} - \theta_{Actual}}{\theta_{Actual}} \right| \times 100 \tag{23}$$

As it can be seen in Table 8, the error of estimation is very close and the accuracy of both RLS and Kalman filter is similar.

For more evaluation, we applied 1739 scenarios of internal fault with/without CT saturation to the RLS and Kalman filter based algorithm. Table 9 provides the accuracy of the both estimators from accuracy and response time aspects.

As it can be seen in Table 9, considering different inception fault angle, fault type, and noise condition, the performance of the both algorithms are almost similar with slight supremacy of the RLS algorithm.

However, it should be mentioned that the main idea of this paper is to employ distance of phase angles of both CTs to distinguish the internal fault and to prevent the mal-operation during inrush current or internal fault accompanied by the CT saturation. To reach fast decision making, the RLS algorithm is employed to provide fast parameter estimation. Nevertheless, the similar parameter estimator like RLS with similar or even better performance can be used instead of RLS but it does not affect the main novelty of this paper.

6. Conclusion

Owning to large differential currents, the inrush current phenomenon may lead to differential protection to mal-operation which may result in power transformer interruption. In this paper, an algorithm based on the MRLS and NMR was designed to discriminate internal faults and inrush currents. The main idea of this algorithm has been established on the fact that during an internal fault, the phase angles of both CT's currents are constant and almost the same. However, in the case of inrush or external faults, the phase angles either are not constant or not the same (i.e. 180° out of phase in the case of external fault).

Applying several simulation and experimental data, it was observed that the PDI is able to identify internal fault signals even in the case of CT saturation within less than a quarter of a cycle. This ability of the PDI is established on the waveform reconstruction from unsaturated interval samples. As a result, the proposed method has low response delay and simultaneously high accuracy even in the case of internal fault accompanied by deep CT saturation. In the case of inrush signals, the PDI can recognize inrush signals even in the case of remnant flux. Proposed method is also able to successfully detect internal faults during transformer energization. Furthermore, the proposed algorithm has immunity during external fault conditions. The comparisons between PDI and with the state-of-the-art algorithms reveal high precision and fast response even in noisy conditions. Therefore, the proposed method is applicable for the discrimination of internal faults and inrush currents.

CRediT authorship contribution statement

Mohsen Tajdinian: Investigation, Conceptualization, Methodology, Supervision, Software, Writing – original draft, Writing – review & editing, Data curation, Visualization, Validation, Formal analysis. **Haidar Samet:** Project administration, Supervision, Writing – original draft, Writing – review & editing, Data curation, Visualization. **Ziad M. Ali:** Project administration, Supervision, Writing – original draft, Validation.

Declaration of Competing Interest

The authors declare that they have no known competing financial interests or personal relationships that could have appeared to influence the work reported in this paper.

Appendix

The specifications of the test system and CTs shown in Fig. 2. are given in Tables 10 and 11 and Fig. 18. Respectively [27].

References

[1] Horowitz SH, Phadke AG. Power System Relaying. 3rd Edition. John Wiley & Sons; 2008.
[2] Liu P, Chen D, Guo Y, Malik OP, Hope GS. Improved operation of differential protection of power transformers for internal faults. IEEE Trans Power Deliv 1992; 7:1912–9.
[3] Hamedani Golshan ME, Saghaian-nejad M, Saha A, Samet H. A new method for recognizing internal faults from inrush current conditions in digital differential protection of power transformers. Electr Power Syst Res 2004;71(1):61–71.
[4] Phadke AG, Thorp JS. A new computer-based flux-restrained curretn-differential relay for power transformer protection. IEEE Trans. Power Appar. Syst. PAS 1983; 102:3624–9.
[5] Kang YC, Lee BE, Kang SH. Transformer protection relay based on the induced voltages. Int J Electr Power Energy Syst 2007;29(4):281–9.
[6] Mostafaei M, Haghjoo F. Flux-based turn-to-turn fault protection for power transformers. IET Gener Transm Distrib 2016;10(5):1154–63.
[7] Inagaki K, Higaki M, Matsui Y, Kurita K, Suzuki M, Yoshida K, et al. Digital protection method for power transformers based on an equivalent circuit composed of inverse inductance. IEEE Trans. Power Deliv. 1988;3(4):1501–10.
[8] Baoming G, deAlmeida AT, Qionglin Z, Xiangheng W. An equivalent instantaneous inductance-based technique for discrimination between inrush current and internal faults in power transformers. IEEE Trans. Power Deliv. 2005;20(4):2473–82.
[9] Zaman MR, Rahman MA. Experimental testing of of artificial neural network based protection of power transformer. IEEE Trans. Power Deliv. 1998;13:510–7.
[10] Moravej Z, Vishwakarma DN, Singh SP. Application of radial basis function neural network for differential relaying of a power transformer. Comput Electr Eng 2003; 29(3):421–34.
[11] Tripathy M, Maheshwari RP, Verma HK. Application of probabilistic neural network for differential relaying of power transformer. IET Gener Transm Distrib 2007;1(2):218. https://doi.org/10.1049/iet-gtd:20050273.
[12] Balaga H, Gupta N, Vishwakarma DN. GA trained parallel hidden layered ANN based differential protection of three phase power transformer. Int J Electr Power Energy Syst 2015;67:286–97.
[13] Wiszniewski A, Kasztenny B. A multi-criteria differential transformer relay based on fuzzy logic. IEEE Trans. Power Deliv. 1995;10(4):1786–92.
[14] Shin M, Park C, Kim J. Fuzzy logic-based relaying for large power transformer protection. IEEE Trans. Power Deliv. 2003;18:718–24.
[15] Gomez-Morante M, Nicoletti DW. A wavelet-based differential transformer protection. IEEE Trans. Power Deliv. 1999;14(4):1351–8.
[16] Eissa MM. A novel digital directional transformer protection technique based on wavelet packet. IEEE Trans. Power Deliv. 2005;20(3):1830–6.
[17] Saleh SA, Scaplen B, Rahman MA. A new implementation method of waveletpacket-transform differential protection for power transformers. IEEE Trans Ind Appl 2011;47(2):1003–12.
[18] Guillén D, Esponda H, Vázquez E, Idárraga-Ospina G. Algorithm for transformer differential protection based on wavelet correlation modes. IET Gener Transm Distrib 2016;10(12):2871–9.
[19] Roy A, Singh D, Misra RK, Singh A. Differential protection scheme for power transformers using matched wavelets. IET Gener Transm Distrib 2019;13(12): 2423–37.
[20] Ali E, Helal A, Desouki H, Shebl K, Abdelkader S, Malik OP. Power transformer differential protection using current and voltage ratios. Electr Power Syst Res 2018; 154:140–50.
[21] Ali E, Malik OP, Abdelkader S, Helal A, Desouki H. Experimental results of ratios - based transformer differential protection scheme. Int Trans Electr Energ Syst. 2019;e12114:1–14.
[22] Ali E, Malik OP, Knight A, Abdelkader S, Helal A, Desouki H. Ratios-based universal differential protection algorithm for power transformer. Electr Power Syst Res 2020;186:106383. https://doi.org/10.1016/j.epsr.2020.106383.
[23] Zhang LL, Wu QH, Ji TY, Zhang AQ. Identification of inrush currents in power transformers based on higher-order statistics. Electr Power Syst Res 2017;146: 161–9.
[24] Weng H, Wang S, Lin X, Li Z, Huang J. A novel criterion applicable to transformer differential protection based on waveform sinusoidal similarity identification. Int J Electr Power Energy Syst 2019;105:305–14.
[25] Weng H, Wang S, Wan Yi, Lin X, Li Z, Huang J. Discrete Fréchet distance algorithm based criterion of transformer differential protection with the immunity to saturation of current transformer. Int J Electr Power Energy Syst 2020;115:105–14.
[26] Zheng T, Huang T, Ma Y, Zhang Z, Liu L. Histogram-based method to avoid maloperation of transformer differential protection due to current-transformer saturation under external faults. IEEE Trans Power Delivery 2018;33(2):610–9.
[27] Tajdinian M, Allahbakhshi M, Bagheri A, Samet H, Dehghanian P, Parkash Malik Om. An enhanced sub-cycle statistical algorithm for inrush and fault currents classification in differential protection schemes. Int J Electr Power Energy Syst 2020;119:105939. https://doi.org/10.1016/j.ijepes.2020.105939.
[28] Phadke AG, Thorp JS. Computer relaying for power systems. John Wiley & Sons; 2009.
[29] Ljung L, Soderstrom T. Theory and Practice of Recursive Identification. Boston: MIT Press; 1999.
[30] Mahanta P, Ahmed HA, Bhattacharyya DK, Kalita JK. An effective method for network module extraction from microarray data. BMC Bioinf 2012;13(13):1–11.
[31] Otsu N. A threshold selection method from gray-level histograms. IEEE Trans Syst Man Cybernetics 1979;9(1):62–6.
[32] Claser R, Nascimento VH. Low-complexity approximation to the Kalman filter using convex combinations of adaptive filters from different families. In: In 2017 25th European Signal Processing Conference (EUSIPCO); 2017. p. 2630–3.